SAND2019-8118J

Structure-Thermodynamics Relationship of Schoepite: A First-Principles Study

Philippe F. Weck,[1,*] Carlos Jové-Colón,[1] and Eunja Kim[2]

[1] *Sandia National Laboratories, Albuquerque, NM 87185, USA*

[2] *Department of Physics and Astronomy, University of Nevada Las Vegas, Las Vegas, NV 89154, USA*

(Dated: July 12, 2019)

The relationship between the structure and thermodynamic properties of schoepite, an important uranyl phase formed upon corrosion of UO_2, has been investigated within the framework of density functional perturbation theory (DFPT). Experimental crystallographic lattice parameters are reproduced within less than ∼0.4% in this study using standard DFT. Phonon calculations within the quasi-harmonic approximation predict standard molar entropy and isobaric heat capacity of $S^0 = 179.60$ J mol^{-1} K^{-1} and C_P^0 =157.4 J mol^{-1} K^{-1} at 298.15 K, i.e., ∼6% and ∼4% larger than existing DFPT-D2 calculations, which appear to overconstrain the attractive interaction between adjacent uranyl layers as a result of the semiempirical dispersion correction term utilized in this method. The computed variation of the standard molar isobaric heat capacity with water content from schoepite ($UO_3 \cdot x H_2O$, $x = 2.25$) to dehydrated schoepite ($x = 1.00$) is predicted to be essentially linear along isotherms ranging from 100 to 500 K. These findings have important implications for the dehydration of layered uranyl corrosion phases and hygroscopic materials.

PACS numbers:

I. INTRODUCTION

The matrix of UO_2-type spent nuclear fuel (SNF) is mostly made of metal oxides materials prone to redox corrosion and dissolution, which is pervasive and of critical importance for environmental systems[1]. Oxidative dissolution of uranium dioxide results mainly in the formation of uranyl phases, which are primarily oxide hydrates, along with silicates, phosphates and carbonates, depending on the local natural system environment utilized for spent fuel storage or disposal. Over fifty uranyl minerals/phases can occur in nature or as SNF corrosion products.

An accurate knowledge of the thermodynamic parameters for uranyl corrosion phases is crucial to predict their stability and behavior, as they may play a role in the degradation of SNF stored in of geological repositories or in the context of nuclear reactor accidents or in the paragenesis of complex assemblage of uranyl minerals in oxidized uranium deposits[2–9]. However, numerous thermodynamic data gaps and research needs exist for uranyl corrosion phases. Accurate thermodynamic data (e.g., heat capacity, entropy,...) obtained from calorimetric experiments are especially scarce or inexistent for schoepite ($[(UO_2)_8O_2(OH)_{12}]\cdot 12H_2O$), metaschoepite ($[(UO_2)_8O_2(OH)_{12}]\cdot 10H_2O$), dehydrated schoepite ($UO_2(OH)_2$), studtite ($((UO_2)O_2(H_2O)_4)$) or metastudtite ($((UO_2)O_2(H_2O)_2)$). Such phases, formed upon exposure of SNF to mixtures of $H_2O + H_2O_2$ or high concentration of H_2O_2 produced by α-radiolysis of water[10,11], are considered of importance[2–8].

Schoepite is of particular significance, since it appears among the most thermodynamically stable corrosion products formed upon alteration of UO_2-type fuel. The structural relationships and transformations among schoepite and its main byproducts, metaschoepite and dehydrated schoepite, were reviewed in details by Finch et al.[9] In contrast, extremely limited information on the thermodynamic properties of these minerals/phases is available in the literature, owing to the difficulty of the calorimetric experiments involving uranyl minerals and compounds[12]. This stems in part from the difficulty to control hydration level in high-temperature calorimetric experiments, leading often to inadvertently interchange schoepite and metaschoepite experimental characterization in previous studies[13,14]. In addition, X-ray diffraction (XRD) investigations carried out to date have yet to fully solve the structure of schoepite[9,15,16]. Finch et al. showed that one-sixth of the interlayer H_2O from schoepite can be lost, leading to the schoepite (space group $P2_1ca$) to metaschoepite (space group $Pbna$) transformation, accompanied by a significant reorganization of H-bonds and a unit-cell volume decrease of ∼3%[9].

In this context, first-principles calculations based on density functional theory (DFT) can provide much needed insights into the structure-thermodynamics relationship of these complex uranyl corrosion phases, as shown in recent studies[17–25]. Using DFT, Ostanin and Zeller originally proposed a schoepite crystal structure[17]. However, due to the resource-intensive nature of these calculations, only half the unit cell ($a \times b \times c/2$) was relaxed, by assuming that adjacent U–O layers only interact weakly through the separating water layer. Their schoepite unit-cell (space group $P2_1$), obtained by doubling the lattice parameter $c/2$ of their optimized simulation cell, has a volume of 3627 Å^3, i.e., ∼2% larger than the equilibrium volume of 3551 Å^3 measured from XRD. Recently, Colmenero et al. proposed a new unit-cell structure of schoepite optimized with DFT[23]. Their calculations included a semiempirical dispersion correction implemented in the DFT-D2 method[26] to account for dispersion forces in the structure of schoepite. As a result, their optimized unit-cell structure is characterized by a volume of 3474.9 Å^3 (space group $P2_1ca$), i.e.,

smaller than experiment by ∼2%. Using this optimized structure, Colmenero et al. derived the thermodynamics of schoepite[25]. Although, both the studies of Ostanin and Zeller and Colmenero et al. utilized the CASTEP code with the same exchange correlation (XC) functional, DFT equilibrium volumes predicted for schoepite either underestimate or overestimate the experimental value by ±2%. While relatively small, such structural differences may impact the accuracy of the overall thermodynamic properties of schoepite predicted form first-principles.

In this study, the structure-thermodynamics relationship of schoepite has been investigated from first-principles using a methodology successfully tested and validated to predict the structures and thermal properties of dehydrated schoepite, studtite and metastudtite[19–22]. The optimized crystal structure of schoepite has been systematically compared with the previous DFT studies of Ostanin and Zeller[17] and Colmenero et al.[23] and the XRD data from Finch et al.[9,15]. In addition, the thermal variations of the molar entropy, bulk modulus, Gibbs free energy, isochoric and isobaric heat capacities, and enthalpy and Gibbs energy functions have been predicted and compared to available experimental data and first-principles results. Details of our computational methods are given in Sec. II, followed by a discussion of our results in Sec. III. A summary of our findings and conclusions is given in Sec. IV.

II. COMPUTATIONAL METHODS

Total-energy calculations were conducted using spin-polarized DFT implemented in the Vienna *Ab initio* Simulation Package (VASP)[27,28]. The XC energy was calculated using the generalized-gradient approximation[29] (GGA) with the parameterization of Perdew, Burke, and Ernzerhof[30] (PBE), similar to the schoepite studies of Ostanin and Zeller[17] and Colmenero et al.[23,25]. The PBE XC functional was also successfully used to calculate the thermodynamic properties of dehydrated schoepite, studtite and metastudtite[20,22]. Although corrections for strong electron correlations between U(IV) $5f$ electrons are necessary in first-principles modeling of bulk UO_2[31], standard DFT was found to accurately describe the structure-properties relationship of periodic systems made of U(VI) building blocks[17,18,20,22,23,25].

The Projector Augmented Wave (PAW) method[32,33] was utilized to represent the interaction between valence electrons and ionic cores. In the Kohn-Sham (KS) equations, O($2s, 2p$) and U($6s, 6p, 6d, 5f, 7s$) electrons were treated as valence states and PAW pseudopotentials were used to describe the remaining core electrons together with the nuclei. A plane-wave cutoff energy of 700 eV was used for the electronic wavefunctions, ensuring total-energy convergence to within 1 meV/atom. The KS equations were solved using the blocked Davidson iterative matrix diagonalization scheme followed by the residual vector minimization method[34]. Methfessel-Paxton Fermi-level smearing[35] with a width set to 0.1 eV for wavefunction partial occupancies was utilized in electronic relaxation calculations.

Ionic and cell relaxation calculations were conducted simultaneously, without symmetry constraints applied, using as starting geometry the 344-atom periodic unit cell (space group $P2_1ca$, IT No. 29, with formula unit $[(UO_2)_8O_2(OH)_{12}]\cdot 12H_2O$ ($Z = 4$) or $UO_3\cdot 2.25H_2O$ ($Z = 32$)) recently proposed by Colmenero et al.[23]. Due to the large size of the simulation cell, calculations were carried out at the center of the Brillouin zone (Γ-point). In initial relaxation calculations, Hellmann-Feynman forces acting on atoms were calculated with a convergence tolerance set to 0.01 eV/Å. Using optimized structures obtained from total-energy minimization near equilibrium volume, successive relaxations with respect to Hellmann-Feynman forces were conducted with more a stringent convergence of 0.001 eV/Å. Phonon properties for these structures were obtained using the linear response method, which used density functional perturbation theory (DFPT) to calculate forces. The thermal properties of bulk schoepite were derived from phonon calculations near equilibrium within the quasi-harmonic approximation (QHA).

III. RESULTS AND DISCUSSION

A. Crystal structure

In agreement with XRD characterization by Finch et al.[9,15,16], the equilibrium crystal unit cell of schoepite relaxed in this study with DFT at the GGA/PBE level of theory crystallizes in the space group $P2_1ca$ (IT No. 29, $Z = 4$). As shown in Fig. 1, all U atoms are coordinated by seven anions in pentagonal bipyramidal arrangements, with U-atom coordination of $UO_2(OH)_5$ or $UO_2O(OH)_4$.

The crystal unit-cell parameters of schoepite optimized in this DFT/PBE study using the VASP code are summarized in Table I, along with the CASTEP DFT/PBE results by Ostanin and Zeller[17] and Colmenero and coworkers[23] and with the corresponding experimental powder XRD parameters[9,15]. The equilibrium lattice parameters predicted in this study are $a = 14.389$ Å, $b = 16.870$ Å, and $c = 14.726$ Å, in excellent agreement with the values of $a = 14.337$ Å, $b = 16.813$ Å, $c = 14.731$ Å measured from powder XRD. Compared to experiment, the calculated in-plane lattice parameters a and b are slightly overestimated by +0.36% and +0.34%, respectively, while the computed c parameter normal to the uranyl layers essentially reproduces experiment (−0.03%). The predicted volume of 3574.9 Å^3 is only +0.67% larger than the experimental value of 3551(2) Å^3. This slight overestimation of lattice parameters is expected, as it stems from the well-known tendency of the GGA/PBE exchange correlation functional to overestimate bond distances. The lattice parameters a and

TABLE I. Crystal unit-cell parameters of schoepite optimized with DFT at the GGA/PBE level of theory and corresponding experimental powder XRD parameters. Percentages given between parentheses indicate the differences relative to the corresponding XRD values.

	a(Å)	b(Å)	c(Å)	c/a	b/a	V(Å^3)	ρ(g/cm^3)	Space group
DFT[a]	14.389	16.870	14.726	1.023	1.172	3574.9	4.854	$P2_1ca$
	(+0.36%)	(+0.34%)	(−0.03%)			(+0.67%)		
DFT[b]	14.387	16.893	14.924	1.037	1.174	3627.1	4.784	$P2_1$
	(+0.34%)	(+0.48%)	(+1.31%)			(+2.14%)		
DFT[c]	14.274	16.808	14.484	1.015	1.177	3474.9	4.994	$P2_1ca$
	(−0.44%)	(−0.03%)	(−1.68%)			(−2.14%)		
Expt.[d]	14.337(3)	16.813(5)	14.731(4)	1.027	1.173	3551(2)	4.886	$P2_1ca$

[a] VASP/DFT, PAW pseudopotentials; this study.
[b] CASTEP/DFT, ultrasoft Vanderbilt pseudopotentials, with $a \times b \times c/2$ cell; Ref. [17].
[c] CASTEP/DFT-D2, norm-conserving pseudopotentials; Ref. [23].
[d] Powder XRD; Refs. [9 and 15].

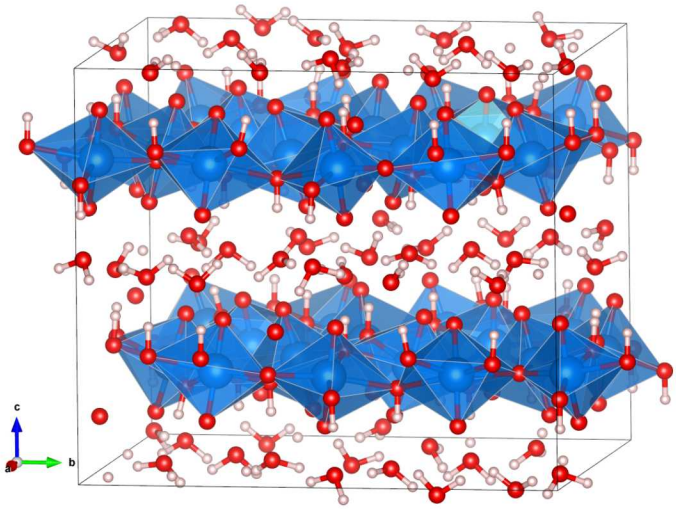

FIG. 1. (Color online) Crystal unit cell of schoepite, $[(UO_2)_8O_2(OH)_{12}]\cdot 12H_2O$ (space group $P2_1ca$, IT No. 29, $Z = 4$), relaxed in this study with DFT at the GGA/PBE level of theory. Color legend: H, white; O, red; U, blue. Uranium coordination polyhedra are shown in blue.

b predicted in this work are also consistent with values of a = 14.387 Å (+0.34% larger than XRD) and b = 16.893 Å (+0.48% larger than XRD) calculated by Ostanin and Zeller using half the unit cell $a \times b \times c/2$. However, their predicted c parameter of 14.924 Å overestimates experiment by +1.31%, resulting in an optimized unit cell +2.14% larger than the volume characterized by XRD. This contrasts with the volume of 3474.9 Å^3 computed by Colmenero and coworkers, which underestimates experiment by −2.14%. While all three lattice parameters appear to underestimate XRD values, their computed c parameter normal to the uranyl layers shows the largest discrepancy with experiments (−1.68%). It can be inferred that the DFT-D2 method is responsible for this discrepancy by using a semiempirical dispersion correction term that overconstrains the attractive interaction between adjacent layers. Previous first-principles DFT-D calculations for dehydrated schoepite[20] showed that there is very limited benefit in using dispersion-corrected DFT and/or DFT+U for this class of systems. Previous computational studies of hydrogen-bonded interactions showed that uncorrected DFT using the PBE XC functional exhibits better performance than DFT-D-type counterparts[36]. Standard DFT was also found to correctly describe the structures and properties of studtite and metastudtite in previous studies[18,19,21,22]. As shown in Table I, among all DFT calculations carried out to date for schoepite, the structure optimized in this study is in closest overall agreement with XRD parameters.

B. Thermodynamic properties

For the sake of consistency with the DFT calculations from Colmenero et al.[25], all the schoepite thermodynamic results discussed below are given relative to a formula unit (f.u.) defined as $UO_3\cdot 2.25H_2O$ (i.e., in such a way that schoepite with formula $[(UO_2)_8O_2(OH)_{12}]\cdot 12H_2O$ ($Z = 4$) is equivalent to $UO_3\cdot 2.25H_2O$ ($Z = 32$)).

Thermodynamics calculations were conducted in this study up to ∼550 K (275 °C), i.e., in the vicinity of the upper limit considered to be the maximum temperature reached at the SNF waste package outer surface during disposal. It is also worth mentioning that early thermal gravimetric analysis (TGA) by Dawson et al.[37] reported that schoepite dehydrates to $UO_3\cdot 0.8H_2O$ between 293 and 413 K. Regarding the the dehydration byproducts of schoepite, previous calorimetric studies showed that metaschoepite is thermally stable to 425 K[13] and that dehydrated schoepite corresponds to compositions of $UO_3\cdot 0.75H_2O$ up to ∼450 K[38] and $UO_3\cdot 0.77H_2O$ up to *ca.* 500 K[39].

As outlined in the computational methods section, the

structure of schoepite optimized in this study was used to derive its bulk thermal properties calculated from phonon frequencies at constant equilibrium volume at the DFPT/PBE level of theory.

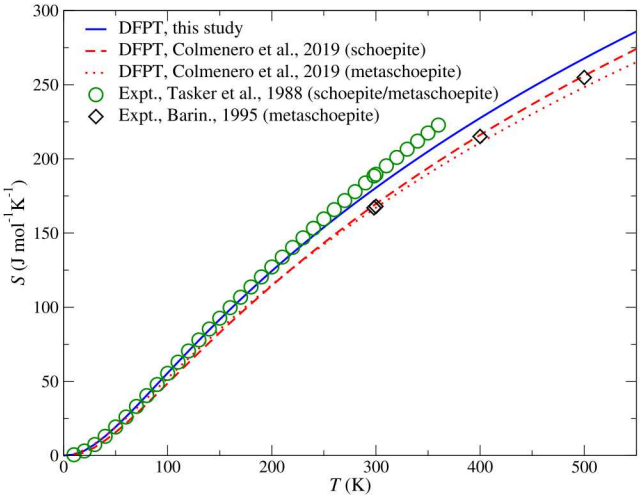

FIG. 2. (Color online) Molar entropy of schoepite calculated at constant equilibrium volume at the DFPT/PBE level of theory. The entropy of schoepite and metaschoepite predicted with DFPT-D2 in Ref. [25] are also shown, along with experimental predictions for schoepite/metaschoepite in Refs. [13 and 40].

The molar entropy, S, was computed as:

$$S = -k_{\mathrm{B}} \sum \ln\left[1 - e^{-\beta\hbar\omega}\right] - \frac{1}{T} \sum \frac{\hbar\omega}{e^{\beta\hbar\omega} - 1}, \qquad (1)$$

where k_{B} is Boltzmann's constant, $\beta = (k_{\mathrm{B}}T)^{-1}$ and T is the temperature of the system, $\hbar$ is Planck's reduced constant, and $\hbar\omega$ is the energy of a single phonon with angular frequency ω. As depicted in Figure 2, the molar entropy calculated here is systematically larger than the results predicted by Colmenero et al. for schoepite. At 298.15 K, a difference of ∼6% is obtained between the value of S^0 = 179.60 J mol^{-1} K^{-1} calculated here and the corresponding value of 168.75 J mol^{-1} K^{-1} computed by Colmenero et al. It can be inferred that this difference stems in part from the variation in density between the structure optimized by Colmenero et al. (ρ = 4.994 g/cm^3) and the one relaxed in this study (ρ = 4.854 g/cm^3), since the entropy increases with unit-cell volume. This is consistent with the fact that a unit-cell volume increase produces a larger number of microstates in the system, W, which in turn increases logarithmically the entropy according to Boltzmann's entropy formula, $S = k_{\mathrm{B}}.\log W$.

The molar entropy obtained by Tasker et al.[13] from calorimetric experiments on synthetic schoepite, with an approximate formula of $UO_3 \cdot 2H_2O$, is also displayed in Fig. 2. This phase was found to have identical XRD patterns to those of the orthorhombic *Pbna* β-$UO_3 \cdot 2H_2O$ product (i.e., synthetic metaschoepite) characterized by Debets and Loopstra[41], although no explicit XRD data were reported by Tasker et al.[13]. As discussed by Finch et al.[9], schoepite and metaschoepite are difficult to distinguish on the basis of XRD patterns alone, and the name schoepite is commonly applied in the literature to synthetic products with chemical compositions close to $UO_3 \cdot 2H_2O$. Moreover, the standard synthetic route used to produce the sample characterized by Tasker et al.[13,37] commonly leads to mixtures of schoepite and metaschoepite[9,16]. As shown in Fig. 2, the molar entropy calculated in this study is in good agreement with the data from Tasker et al. up to ∼180–200 K, while the DFPT prediction at 298.15 K underestimates the corresponding experimental value by less than ∼5%. The larger experimental values above ∼200 K might be the onset of the sluggish phase transformation between schoepite → metaschoepite or between schoepite/metaschoepite → dehydrated schoepite, which starts around 293 K according to the TGA investigation of Dawson et al.[37]. It is interesting to note that, as expected, the entropy reported by Barin[40] for pure metaschoepite is consistently smaller than the present DPFT predictions for schoepite and the schoepite/metaschoepite data from Tasker et al.[13]. For the sake of comparison, the DFPT-D2 results of Colmenero et al.[25] for metaschoepite have been represented in Fig. 2; their computed entropy of schoepite is ∼1.5% larger than that of metaschoepite at 298.15 K.

The thermal properties of schoepite at standard pressure (1 bar) were predicted within the QHA by conducting a series of DFPT calculations near equilibrium. At constant hydrostatic pressure P, the Gibbs free energy, G, was obtained by the following transformation to introduce a volume dependence[42]:

$$G(T,P) = \min_{\mathrm{V}} \left[U(V) + F_{\mathrm{phonon}}(T;V) + PV\right], \qquad (2)$$

where $\min_{\mathrm{V}}$[function of V] corresponds to a unique minimum of the expression between brackets with respect to the unit-cell volume V, $U(V)$ is the total energy of the system, and the phonon contribution is

$$F_{\mathrm{phonon}}(T;V) = \frac{1}{2} \sum \hbar\omega + k_{\mathrm{B}}T \sum \ln\left[1 - e^{-\beta\hbar\omega}\right]. \qquad (3)$$

The thermodynamic functions of Eq. (2) were fitted to the universal Vinet equation of state[43]:

$$P(V) = 3K_0 \frac{(1-x)}{x^2} \exp\left[\frac{3}{2}(K_0' - 1)(1-x)\right], \qquad (4)$$

where $x = (V/V_0)^{1/3}$, V_0 and V are the equilibrium and deformed unit-cell volumes, respectively, the bulk modulus is

$$K_0(T) = -V \left(\frac{\partial P}{\partial V}\right)_{P=0}, \qquad (5)$$

and K_0' is its derivative with respect to the pressure. As shown in Figure 3, the bulk modulus computed with the Vinet EOS with DFPT/QHA decreases monotonically from $K_0 = 31.6$ GPa in the athermal limit to $K_0 = 11.9$ GPa at 550 K, thus exhibiting the typical Anderson-Grüneisen temperature dependence of elastic moduli of oxide compounds[44]. This single-cystal athermal value is in line with the corresponding value of $K_0 = 35.17$ GPa predicted with DFT/PBE by Colmenero et al. using a fourth-order Birch-Murnaghan EOS[23], as well as with the value of $K_0 = 36.3$ GPa obtained from the Vinet EOS fit to the DFT/PBE cold curve computed in this study.

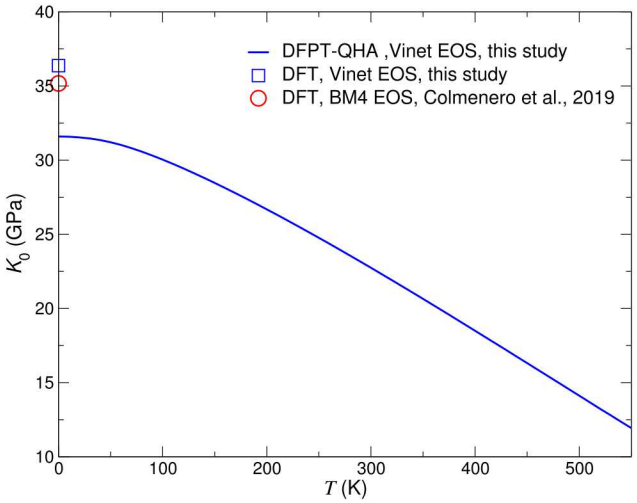

FIG. 3. (Color online) Thermal evolution of the bulk modulus K_0 for schoepite calculated using the Vinet equation of state (EOS) with DFPT/PBE within the QHA. The athermal bulk modulus values predicted from DFT/PBE in Ref. [25] using the fourth-order Birch-Murnaghan EOS and in this study using the Vinet EOS are also represented.

The thermal variations of the Gibbs free energy and the isobaric molar heat capacity, C_P, at constant atmospheric pressure are shown in Figures 4 and 5, respectively. The isobaric molar heat capacity, C_P, was computed as the second derivative of the Gibbs free energy from Eq. (2) with respect to the temperature:

$$C_P(T,P) = -T\frac{\partial^2 G(T,P)}{\partial T^2}. \quad (6)$$

Density of states calculations carried out in this investigation predicted that schoepite is a semiconductor with a band gap of 1.5 eV. Therefore, no electronic contribution needs to be added to the vibrational heat capacity of Eq. (6).

The standard value calculated at 298.15 K in this study was C_P^0 =157.4 J mol^{-1} K^{-1}, which is ∼4% larger than the value of 150.62 J mol^{-1} K^{-1} computed by Colmenero et al.[25]. Significantly larger differences of up to ∼11% are found at higher temperature, where the heat capacity was predicted to reach 212.54 J mol^{-1} K^{-1} at 550 K in

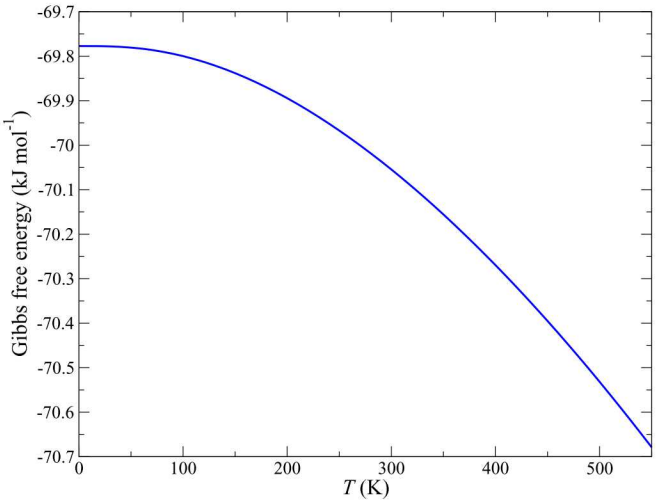

FIG. 4. (Color online) Gibbs free energy of schoepite at constant atmospheric pressure computed at the DFPT/PBE level of theory.

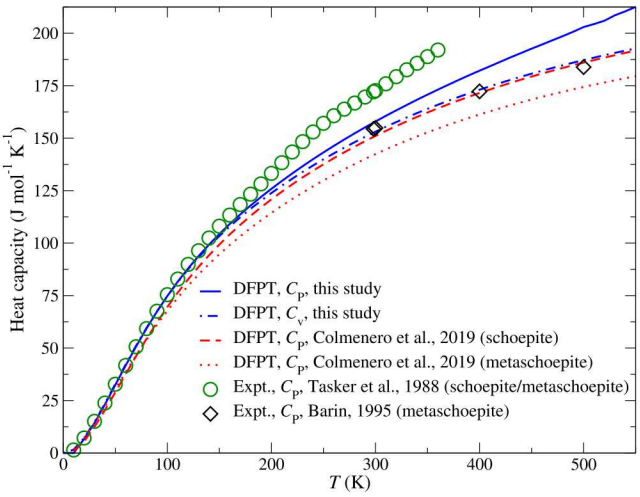

FIG. 5. (Color online) Isobaric (C_P) and isochoric (C_V) molar heat capacity of schoepite at constant atmospheric pressure computed at the DFPT/PBE level of theory. The C_P for schoepite and metaschoepite predicted with DFPT-D2 in Ref. [25] are also displayed, along with calorimetric measurements for schoepite/metaschoepite in Refs. [13 and 40].

this investigation. This value of the heat capacity is well below the Dulong-Petit asymptotic value of schoepite, i.e., $C_P = n.3R = 268.1$ J mol^{-1} K^{-1}, where n is the number of atoms per f.u. ($n = 10.75$ for $UO_3 \cdot 2.25H_2O$) and $R = 8.314$ J mol^{-1} K^{-1} is the universal gas constant. Let us note that the value of $C_P = 223.2$ J mol^{-1} K^{-1} predicted at 1000 K by Colmenero et al. is still ∼17% below the Dulong-Petit limit. Although data exist for

metaschoepite[13], to the best of our knowledge, no experimental heat capacity data are available for schoepite. As observed for the entropy, noticeable differences appear above ∼180 K between the C_P predicted in this study and the calorimetric data of Tasker et al.[13], possibly due to the presence of schoepite → metaschoepite and/or schoepite/metaschoepite → dehydrated schoepite phase transitions[37], while DFPT predictions closely reproduces experiment below this temperature. For the sake of comparison, the calorimetric data of Barin[40] and the calculations of Colmenero et al.[25] for metaschoepite are also depicted in Fig. 5.

In addition, the isochoric molar heat capacity, C_V, was calculated at equilibrium volume using the expression:

$$C_V = k_B \sum (\beta\hbar\omega)^2 \frac{e^{\beta\hbar\omega}}{[e^{\beta\hbar\omega} - 1]^2}. \quad (7)$$

As represented in Fig. 5, the variation of C_V is close to the C_P calculated for schoepite by Colmenero et al.[25]. This suggests that differences in isobaric heat capacity between both DFPT studies might stem from differences in volume variation near equilibrium, as a result of the semiempirical dispersion correction term used in DFT-D2 calculations.

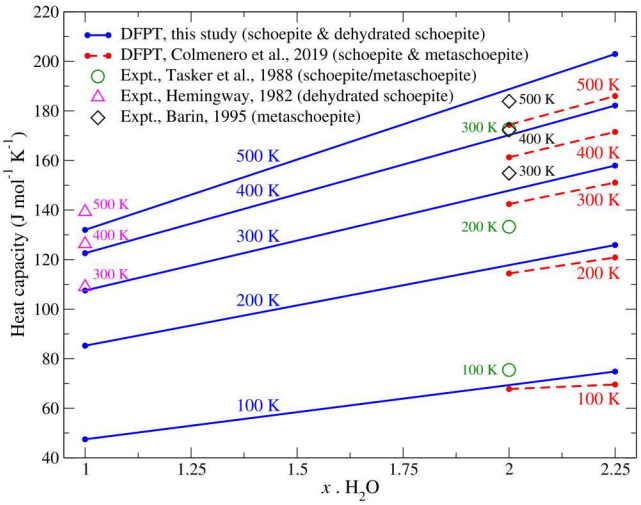

FIG. 6. (Color online) Variation of the isobaric molar heat capacity with water content from schoepite ($UO_3 \cdot xH_2O$, x = 2.25) to dehydrated schoepite (x = 1.00; Ref. [20]) at constant atmospheric pressure computed at the DFPT/PBE level of theory for isotherms between 100 and 500 K (blue). The C_P for schoepite and metaschoepite (x = 2.00) predicted with DFPT-D2/PBE in Ref. [25] are also displayed (red), along with calorimetric measurements for schoepite/metaschoepite in Refs. [13 and 40] and dehydrated schoepite in Ref. [39].

In order to understand the possible impact of interlayer H_2O variation on thermal properties, the evolution of C_P with water content from schoepite to dehydrated schoepite ($UO_3 \cdot xH_2O$, x = 1 − 2.25) at constant atmospheric pressure was represented in Fig. 6 for isotherms ranging from 100 to 500 K. For each isotherm, the C_P variations predicted by Colmenero et al.[25] from schoepite to metaschoepite (in red) are overall qualitatively similar to the variations between values predicted for schoepite in this study and previous DFPT results for dehydrated schoepite obtained with similar methods (in blue)[20]. Moreover, for isotherms between 300 and 500 K, the calorimetric data of Barin[40] for metaschoepite and of Hemingway[39] for dehydrated schoepite appear nearly aligned with the latter DFPT variations from x = 2.25 to x = 1. These findings suggest that the variation of C_P with water content is essentially linear from schoepite to dehydrated schoepite along isotherms.

To obtain the enthalpy and Gibbs energy functions, a nonlinear least-squares regression to a Haas-Fisher-type polynomial was used to fit the the thermal evolution of the isobaric molar heat capacity calculated from DFPT/PBE for bulk shoepite according to:

$$C_P = a + bT + cT^{-2} + dT^{-0.5} + eT^2, \quad (8)$$

The optimized coefficients for Eq. (8) in the temperature range 100−550 K are summarized in Table II. The sum of the squared differences between the present DFPT results and the fit is 1.08, thus suggesting a good correlation between the predicted data and the resulting fit.

TABLE II. Coefficients of the Haas-Fisher heat capacity polynomial $C_P(T)$ for schoepite. The range of validity of the fit is 100–550 K.

$a \times 10^2$ (T^0)	$b \times 10^{-2}$ (T)	$c \times 10^6$ (T^{-2})	$d \times 10^3$ ($T^{-0.5}$)	$e \times 10^{-5}$ (T^2)	SSD[a]
2.1740	11.871	0.132688	-1.67607	-0.144	1.08

[a] Sum of squared differences (SSD) between the calculated and fitted data.

The enthalpy function, $(H_T - H_{298.15})T^{-1}$, was then computed by analytical integration of the fit to the isobaric molar heat capacity using the formula:

$$(H_T - H_{298.15})T^{-1} = \int_{298.15}^{T} C_P(T)\mathrm{d}T, \quad (9)$$

The Gibbs energy function, $(G_T - H_{298.15})T^{-1}$, was calculated using the expression:

$$(G_T - H_{298.15})T^{-1} = (H_T - H_{298.15})T^{-1} - S, \quad (10)$$

where S corresponds to the entropy calculated from Eq. (1). Results for the experimental and computed enthalpy function and Gibbs energy function for bulk schoepite are shown in Figures 7 and 8, along with with previous computational results from Ref. [25].

As shown in Figure 7, the enthalpy function calculated in this study is systematically larger than the previous values reported by Colmenero et al., with differences as large as ∼7% at 550 K, where a value of 85.39 J mol^{-1}

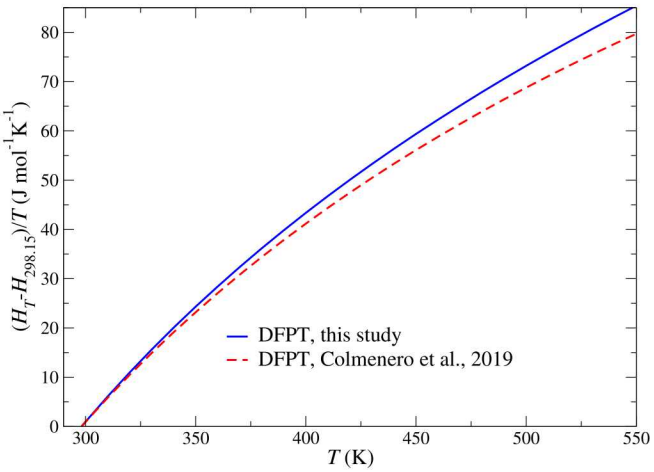

FIG. 7. (Color online) Enthalpy function of schoepite calculated at the DFPT/PBE level of theory. The enthalpy function of schoepite predicted in Ref. [25] is shown as a dashed line.

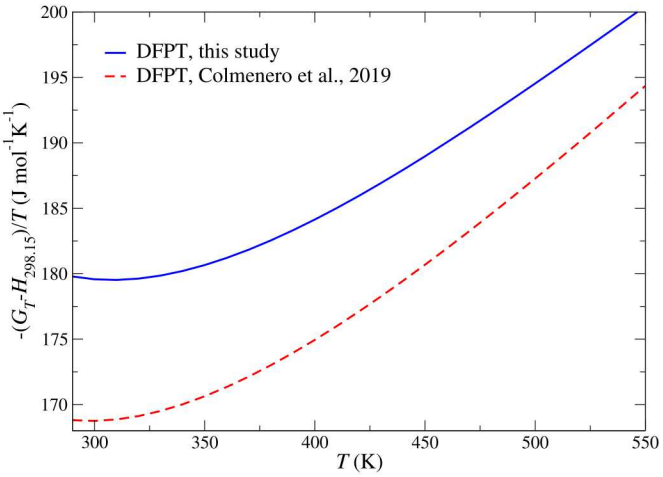

FIG. 8. (Color online) Gibbs energy function of schoepite calculated at the DFPT/PBE level of theory. The Gibbs energy function of schoepite predicted in Ref. [25] is shown as a dashed line.

K^{-1} is calculated in the present study. This is in line with the difference of ∼11% at 550 K found between the isobaric molar heat capacities calculated in both investigations. The calculated Gibbs energy function (see Figure 8) is larger than the DFT predictions of Colmenero et al. by up to ∼6–7% at 298.15 K and ∼3% at 550 K. As discussed above, such discrepancy might be ascribed in part to the use by Colmenero et al. of a DFPT-D2 correction method, which tends to overconstrain the attractive interaction between adjacent layers compared to the structure characterized by XRD.

IV. CONCLUSION

In summary, the relationship between the structure and thermodynamic properties of schoepite has been investigated using DFT/DFPT calculations and systematically compared with existing experimental data and first-principles predictions. The crystal structure relaxed with standard DFT/PBE reproduces experimental lattice parameters within less than ∼0.4%, improving upon previous DFPT-D2 calculation which appear to overconstrain the attractive interaction between adjacent uranyl layers as a result of a semiempirical dispersion correction term.

Phonon calculations using the quasi-harmonic approximation with DFPT predict a molar entropy systematically larger than previous computational results by Colmenero et al., possibly as a results of different equilbrium crystal densities in both studies. The molar entropy calculated in this study is in good agreement with the data from Tasker et al. for schoepite/metaschoepite up to 180–200 K, while at 298.15 K, the entropy is S^0 = 179.60 J mol^{-1} K^{-1}, i.e., ∼5% below the experimental value of Tasker et al. and ∼6% larger than the existing DFPT-D2 prediction. The larger experimental values above ∼200 K might be the onset of the sluggish phase transformation between schoepite → metaschoepite or between schoepite/metaschoepite → dehydrated schoepite, which starts around 293 K according to TGA investigations. The standard isobaric heat capacity calculated at at 298.15 K in this study is $C_{\rm P}^0$ =157.4 J mol^{-1} K^{-1}, i.e., ∼4% larger than existing DFPT-D2 calculations, with signicantly larger differences of up to 11% are found at higher temperature around 550 K. In addition, the variation of the standard molar isobaric heat capacity with water content from schoepite ($UO_3 \cdot x H_2O$, x = 2.25) to dehydrated schoepite (x = 1.00) is predicted to be essentially linear along isotherms ranging from 100 to 500 K, based on DFPT calculations and calorimetric data. The enthalpy function obtained from the computed $C_{\rm P}^0$ is systematically larger than the previous DFPT-D2 values, with differences as large as ∼7% at 550 K. The calculated Gibbs energy function is larger than the DFT predictions of Colmenero et al. by up to ∼6–7% at 298.15 K and ∼3% at 550 K.

The findings discussed in this study have important implications for the dehydration of layered uranyl corrosion phases and hygroscopic materials and similar DFT/DFPT calculations are underway for additional uranyl phases. The present first-principles results also emphasizes the current need for new accurate calorimetric data for uranyl corrosion phases such as schoepite and metaschoepite.

Acknowledgments

Sandia National Laboratories is a multi-mission laboratory managed and operated by National Technology and Engineering Solutions of Sandia, LLC., a wholly owned subsidiary of Honeywell International, Inc., for the U.S. Department of Energy's (DOE) National Nuclear Security Administration under contract DE-NA0003525. This research was performed using funding received from the U.S. DOE, Office of Nuclear Energy's Spent Fuel and Waste Science & Technology (SFWST) R&D Campaign and Nuclear Energy University Program (NEUP). The views expressed in the article do not necessarily represent the views of the U.S. DOE or the United States Government.

* Email: pfweck@sandia.gov

[1] W. Stumm, *Chemistry of the solid-water interface: Processes at the mineral-water and particle-water interface in natural systems* (John Wiley and Sons, Inc., New York, 1992).
[2] K. Kubatko, K. Helean, A. Navrotsky, and P. Burns, Science **302**, 1191 (2003).
[3] P. C. Burns, R. C. Ewing, and A. Navrotsky, Science **335**, 1184 (2012).
[4] X. Guo, S. V. Ushakov, S. Labs, H. Curtius, D. Bosbach, and A. Navrotsky, Proc. Natl. Acad. Sci. USA **111**, 17737 (2014).
[5] C. R. Armstrong, M. Nyman, T. Shvareva, G. E. Sigmon, P. C. Burns, and A. Navrotsky, Proc. Natl. Acad. Sci. USA **109**, 1874 (2012).
[6] B. Hanson, B. McNamara, E. Buck, J. Friese, E. Jenson, K. Krupka, and B. Arey, Radiochimica Acta **93**, 159 (2005).
[7] B. McNamara, B. Hanson, E. Buck, and C. Soderquist, Radiochimica Acta **93**, 169 (2005).
[8] E. C. Buck, R. S. Wittman, C. Z. Soderquist, and B. K. McNamara, RSC Advances **8**, 18227 (2018).
[9] R. J. Finch, F. C. Hawthorne, and R. C. Ewing, Canadian Mineralogist **36**, 831 (1998).
[10] Z. D. Draganic and I. G. Draganic, Journal of Physical Chemistry **75**, 3950 (1971).
[11] G. Sattonnay, C. Ardois, C. Corbel, J. Lucchini, M. Barthe, F. Garrido, and D. Gosset, Journal of Nuclear Materials **288**, 11 (2001).
[12] T. Y. Shvareva, J. B. Fein, and A. Navrotsky, Industrial & Engineering Chemistry Research **51**, 607 (2012).
[13] I. R. Tasker, P. A. G. O'Hare, B. M. Lewis, G. K. Johnson, and E. H. P. Cordfunke, Can. J. Chem. **66**, 620 (1988).
[14] P. A. G. O'Hare, B. M. Lewis, and S. N. Nguyen, The Journal of Chemical Thermodynamics **20**, 1287 (1988).
[15] R. J. Finch, M. A. Cooper, F. C. Hawthorne, and R. C. Ewing, Canadian Mineralogist **34**, 1071 (1996).
[16] R. J. Finch, F. C. Hawthorne, M. L. Miller, and R. C. Ewing, Powder Diffraction **12**, 230 (1997).
[17] S. Ostanin and P. Zeller, Journal of Physics-Condensed Matter **19**, 246108 (2007).
[18] S. Ostanin and P. Zeller, Phys. Rev. B **75**, 073101 (2007).
[19] P. F. Weck, E. Kim, C. F. Jové-Colón, and D. C. Sassani, Dalton Trans. **41**, 9748 (2012).
[20] P. F. Weck and E. Kim, Dalton Trans. **43**, 17191 (2014).
[21] P. F. Weck, E. Kim, and E. C. Buck, RSC Adv. **5**, 79090 (2015).
[22] P. F. Weck and E. Kim, The Journal of Physical Chemistry C **120**, 16553 (2016).
[23] F. Colmenero, J. Cobos, and V. Timón, Inorganic Chemistry **57**, 4470 (2018).
[24] A. M. Colmenero, Fernandez, J. Cobos, and V. Timón, J. Phys. Chem. C **122**, 5268 (2018).
[25] F. Colmenero, A. M. Fernandez, J. Cobos, and V. Timón, ACS Earth and Space Chemistry **3**, 17 (2019).
[26] S. Grimme, Journal of Computational Chemistry **27**, 1787 (2006).
[27] G. Kresse and J. Hafner, Phys. Rev. B **47**, 558 (1993).
[28] G. Kresse and J. Furthmüller, Phys. Rev. B **54**, 11169 (1996).
[29] J. P. Perdew, J. A. Chevary, S. H. Vosko, K. A. Jackson, M. R. Pederson, D. J. Singh, and C. Fiolhais, Phys. Rev. B **46**, 6671 (1992).
[30] J. P. Perdew, K. Burke, and M. Ernzerhof, Phys. Rev. Lett. **77**, 3865 (1996).
[31] P. F. Weck, E. Kim, C. F. Jové-Colón, and D. C. Sassani, Dalton Trans. **42**, 4570 (2013).
[32] P. E. Blöchl, Phys. Rev. B **50**, 17953 (1994).
[33] G. Kresse and D. Joubert, Phys. Rev. B **59**, 1758 (1999).
[34] E. R. Davidson, in *Methods in Computational Molecular Physics*, Vol. 113, edited by G. H. F. Diercksen and S. Wilson (NATO Advanced Study Institute, Series C, Plenum, New York, 1983) p. 95.
[35] M. Methfessel and A. T. Paxton, Phys. Rev. B **40**, 3616 (1989).
[36] K. S. Thanthiriwatte, E. G. Hohenstein, L. A. Burns, and C. D. Sherrill, Journal of Chemical Theory and Computation **7**, 88 (2011).
[37] J. K. Dawson, E. Wait, K. Alcock, and D. R. Chilton, J. Chem. Soc. , 3531 (1956).
[38] H. R. Hoekstra and S. Siegel, J. Inorg. Nucl. Chem. **35**, 761 (973).
[39] B. S. Hemingway, *Thermodynamic properties of selected uranium compounds and aqueous species at 298.15 K and 1 bar and at higher temperatures; preliminary models for the origin of coffinite deposits* (USGS Open-File Report 82-619, 1982).
[40] I. Barin, *Thermochemical Data of Pure Substances* (3rd ed.; VCH Weinheim, 1995).
[41] P. C. Debets and B. O. Loopstra, Journal of Inorganic & Nuclear Chemistry **25**, 945 (1963).
[42] A. Togo, F. Oba, and I. Tanaka, Phys. Rev. B **78**, 134106 (2008).
[43] P. Vinet, J. H. Rose, J. Ferrante, and J. R. Smith, J. Phys. Condens. Matter **1**, 1941 (1989).
[44] O. L. Anderson, Phys. Rev. **144**, 553 (1966).